Earth and Planetary Science Letters 608 (2023) 118086

Contents lists available at ScienceDirect

Earth and Planetary Science Letters

journal homepage: www.elsevier.com/locate/epsl

Two slip regimes in sheared granular fault

Yahui Zhang [a], Ke Gao [a,*], Changdong Li [b,c]

[a] Department of Earth and Space Sciences, Southern University of Science and Technology, Shenzhen, 518055, Guangdong, China
[b] Faculty of Engineering, China University of Geosciences, Wuhan, 430074, Hubei, China
[c] Badong National Observation and Research Station of Geohazards, China University of Geosciences, Wuhan, 430074, China

ARTICLE INFO

Article history:
Received 18 July 2022
Received in revised form 3 February 2023
Accepted 26 February 2023
Available online xxxx
Editor: J.P. Avouac

Keywords:
sheared granular gouge
stick-slip
gouge stress heterogeneity
particle-level contact evolution
coordination number

ABSTRACT

In the stick-slip cycles of faults, the evolving contact state inside the gouge is a major contribution to the evolution of fault friction. However, the microscopic contact changes within stick-slip cycles associated with the possible existence of multiple fault slip regimes are still obscure. By simulating a sheared fault containing a granular gouge, we examine the particle-level contact evolution inside the gouge and the corresponding gouge stress field heterogeneity at fault slip. We find two regimes of fault slip driven by the heterogeneity of the gouge stress field: in the case of weak gouge stress field heterogeneity, local contact rearrangements give rise to macroscopic friction coefficient drop and accumulated gouge stress field heterogeneity (dispersive regime); in the instance of strong stress field heterogeneity, catastrophic failure occurs via contact rearrangement sweeping the whole fault and homogenizes the stress field distribution in the gouge (pervasive regime). In the language of self-organized criticality, the accumulation of gouge stress field heterogeneity is an inevitable consequence of increased entropy in the preparation stage of a large earthquake, which eventually destroys the long-range stress field correlations in the gouge and resets at the beginning of a new cycle of a large earthquake.

1. Introduction

Since stick-slip was proposed as a mechanism for earthquakes (Brace and Byerlee, 1966), attention to earthquake research has been focusing on the frictional instability of faults (Im et al., 2017; Johnson et al., 1973; Kaproth and Marone, 2013; Marone et al., 1990). Laboratory friction experiments revealed that the macroscopic friction coefficient along fault surfaces increases in the "stick" stage and eventually decreases manifested by fault slip, causing the reoccurrence of the rise and drop in fault friction (Byerlee and Brace, 1968; Marone, 1998). Therefore, the earthquake corresponds to the "slip", and the "stick" represents the interseismic period for elastic strain accumulation (Scholz, 1998). By regarding earthquake activities as a series of stick-slip cycles, one might ignore the important aspects of fault evolution, for example, the effect of a slip event on stress redistribution. While a good phenomenological theory may still have decent predictive power, understanding the microscopic evolutionary changes in the stick-slip cycles would reveal the mystery of earthquake recurrence and, more importantly, the possible existence of multiple dynamic regimes in sheared faults. Essentially, the macroscopic friction coefficient reflects the stress field change inside the fault (Gao et al., 2018), while only focusing on the macroscopic friction coefficient is entirely insufficient to deal with such problems involving the evolution of the gouge stress field.

The well-known rate and state friction law (RSF) explains friction as a dependency of sliding velocity and a state variable θ (Dieterich, 1979), which accounts for many phenomena of frictional instability regimes (Helmstetter and Shaw, 2009; Li et al., 2011; Marsan, 2006; Rubin, 2008; Thøgersen et al., 2019). Although the state variable θ can be interpreted in multiple ways (Beeler et al., 1994; Dieterich, 1978, 1979; Nakatani, 2001; Ruina, 1983), it essentially highlights the significant contributions of the time-dependent contact state of fault surfaces to variations in resistance to shear. From a more microscopic point of view, the contact state is the particle-level frictional contact evolution (Falk and Langer, 1998; Kruyt and Rothenburg, 2016; Xing et al., 2021; Zheng et al., 2021). Therefore, it is enlightening that the particle-level contact state, in connection with the stress field evolution inside the gouge, could be a potential candidate to illuminate the evolution of stick-slip dynamics in sheared granular fault.

As a by-product of continuous fault grinding, the granular gouge plays a dominant role in fault strength and stability, thus is genetic to many stick-slip behaviors such as the magnitude of friction drop, reoccurrence time, interseismic frictional healing and the ratio of preseismic slip to dynamic slip (Anthony, 2005; Fer-

* Corresponding author.
E-mail address: gaok@sustech.edu.cn (K. Gao).

https://doi.org/10.1016/j.epsl.2023.118086
0012-821X/

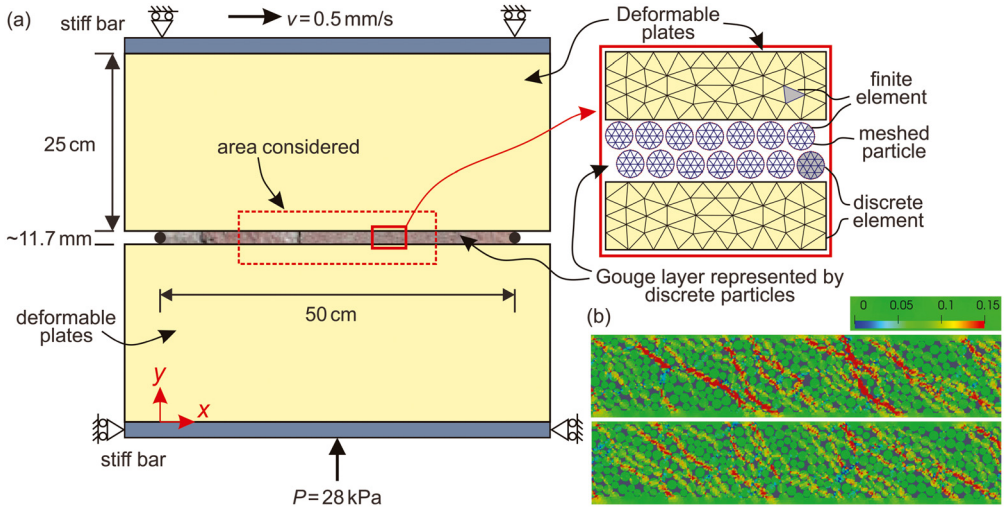

Fig. 1. (a) Numerical representation of the fault containing granular gouge using the combined finite-discrete element method (FDEM). The plate is explicitly represented in FDEM and the gouge layer is composed of a series of discrete particles. Both plates and particles are further discretized into finite elements to capture their deformation and stress field evolution. (b) Comparison of a larger (upper) and smaller (lower) stress field heterogeneity shown by the distribution of stress tensor component τ_{xy} (MPa) in the granular fault gouge (the area considered) immediately before and after a typical fault slip event, respectively.

dowsi et al., 2013, 2014; Johnson et al., 2008). In particular, the granular nature of fault gouge makes it feasible to obtain the microscale information (stress chain network, grain size distribution and grain comminution, granular arrangements, etc.) with the aid of numerical approaches and investigate the connections between fault frictional behavior and gouge particle dynamics. Currently, stick-slip behavior in sheared granular media is commonly simulated using the discrete element method (DEM). (Dorostkar et al., 2017; Ferdowsi et al., 2013; Mair et al., 2002). However, DEM has many apparent limitations. For example, DEM is incapable of capturing detailed deformation and stress distributions within particles and fault blocks; the representation of the shearing plate is often either ignored or simplified by a set of bonded particles; regular shape and unbreakable particles are mainly used in the DEM simulations.

To overcome the restrictions and limitations of DEM, we use a more versatile method – the combined finite-discrete element method (FDEM) – to simulate a two-dimensional (2D) sheared fault system containing a granular gouge, and focus on the particle-level contact behavior and the emergent stress field evolution inside the gouge (homogeneous or heterogeneous) in consecutive stick-slip cycles. We illuminate the nature of gouge stress field heterogeneity in slip events in two regimes: (i) local contact modification results in a more heterogeneous stress field distribution (dispersive regime) in the simulated fault gouge, while (ii) the contact change sweeps through the fault and homogenizes the gouge stress field to a tremendous degree (pervasive regime). In the dispersive regime, the "key contacts" supporting the contact structure are more prone to be rearranged. We speculate that the small interevent slips governed by the dispersive regime may serve as a multi-level preparation process for the abrupt and significant friction drop in the pervasive regime. One implication for the actual seismic activities is that the heterogeneity degree of the gouge stress field correlates well with the consecutive stick-slip cycles.

2. Methods

2.1. Combined finite-discrete element method

The FDEM was originally developed by Munjiza in the early 1990s to simulate the material transition from continuum to discontinuum (Munjiza, 1992). The essence of this method is to merge the algorithmic advantages of discrete element method (DEM) with those of finite element method (FEM). FDEM allows the explicit geometric and mechanical realization of systems involving both continua and discontinua, which makes it superior to pure FEM or DEM. For simulating a fault system containing granular gouge, FDEM is particularly a suitable tool in terms of capturing the deformations of both the granular particles and the shearing plates, as well as the particle-particle and particle-plate interactions (Gao et al., 2018, 2019, 2020). Compared with the rigid particle based DEM widely used for granular fault simulation, FDEM can also directly obtain the detailed stress tensor field evolution inside the gouge, thus making the current analysis of gouge stress field heterogeneity possible.

The main theory of FDEM involves the algorithms of governing equations, deformation description, contact detection, and contact interaction (Lei et al., 2016; Munjiza et al., 2006). It is beyond the scope of the present paper to provide a complete description of the above principles. Details of these can be found in FDEM monographs (Munjiza, 2004; Munjiza et al., 2011, 2014) and our previous papers (Gao et al., 2018, 2019, 2020).

2.2. Numerical model setup

The sheared granular fault system is simulated using FDEM (Gao et al., 2018). Fig. 1 shows the geometry of the model constructed based on a laboratory photoelastic experiment conducted by Geller et al. (2015). To avoid significant model distortion caused by the shearing, two stiff bars are attached to the top and bottom plates. Each plate has dimensions of 570 mm × 250 mm in width and height, respectively. For simplicity, 2D plane stress conditions are assumed.

As we focus on only a segment of the fault to investigate the microscopic dynamics of stick-slips, the overall planar boundaries are adopted to eliminate the influence of fault morphology. The gouge layer in the numerical model consists of a total of 2,817 non-broken circular particles with a bi-modal distribution of particle diameters of 1.2 and 1.6 mm, which are sandwiched between two identical deformable plates. The current particle size distribution is in accordance with the experimental design using nylon rods (Geller et al., 2015) for comparison of the numerical and experimental results. Choosing different particle size distributions can result in various particle contact configurations and stress distributions. While macroscopically speaking, the gouge can be regarded as "homogeneous" upon sufficient number of particles. Ac-

cording to the existing literature on simulations of stick-slip problems (Dorostkar et al., 2017; Ferdowsi et al., 2014), the number of particles adopted is appropriate. Each particle is not perfectly circular (almost circular, see inset of Fig. 1a), but further decomposed into 24 approximately equal size triangle finite elements to capture the deformation of particles as well as the evolution of stress tensors in the gouge. Particle breakage is insignificant under the simulated low normal stress (28 kPa), and thus is excluded in this model. Explicitly simulating particle breakage in FDEM involves remeshing at the expense of high computational cost. The particles are randomly mixed and arranged between the plates in 9 rows and 313 columns before consolidation. The particle-particle and particle-plate friction coefficients are set to 0.15 because a smaller friction coefficient allows for larger slip events and reduces the frequency of small fluctuations in the macroscopic friction signal (Ferdowsi, 2014).

The shear is realized by applying a horizontal velocity $v = 0.5$ mm/s to the top stiff bar, which corresponds to a strain rate $\dot{\varepsilon} = 0.001\ \mathrm{s}^{-1}$. A constant normal load $P = 28$ kPa (vertical direction) is maintained on the bottom stiff bar. The inertial number $I = \frac{\dot{\varepsilon} d}{\sqrt{P/\rho}} \approx 9.0 \times 10^{-6} < 10^{-3}$ (d is the average diameter of particles, $\rho = 1{,}150\ \mathrm{kg/m}^3$ is the particle density), thus ensuring a quasi-static shearing state. The model is run for roughly 2.7×10^8 time steps with a time step of 1.0×10^{-4} ms, corresponding to a total shearing time of approximately 27,000 ms. To avoid edge effects, only the middle section of the gouge containing 1,917 particles (about 340 mm in length) is considered in the present study. These particles are numbered horizontally from left to right and then bottom to top according to their original positions. The shear and normal forces between the particles and the upper and lower plates, as well as the stress tensors of the particles, are recorded every 1 ms. The ratio of the shear to normal force between the plates and granular fault gouge is then calculated as the macroscopic friction coefficient to reflect the stick-slips in the sheared granular fault system. The friction coefficient monotonously increases at the beginning and reaches a plateau after the first 5,000 ms. The main parameters used in the FDEM model are presented in Table S1 of the Supplementary Material.

One should note that various slip regimes in sheared granular fault gouges can be modeled by choosing an appropriate combination of key parameters such as normal pressure, shear velocity, material stiffness and model size. For example, the sheared fault tends to exhibit stable sliding by increasing the shear velocity or decreasing the normal load. As we focus on the stick-slip behavior solely in the current study, the combination of key parameters selected can guarantee the generation of repetitive stick-slip events; while other slip modes are not considered at the moment. A detailed comparison and calibration between the simulated stick-slip events and the laboratory physical experiments have been presented in our earlier work (Gao et al., 2018, 2019, 2020), which shows a good agreement with the laboratory results and generates slip events with magnitudes following the Gutenberg-Richter distribution (Gutenberg and Richter, 1955) (see also Figure S1 in the Supplementary Material). We have attached a supplementary movie showing the kinematics of particle motion during a typical slip event.

2.3. Scalar-valued measure of stress field heterogeneity

During the simulation, we continuously calculate and output the complete stress tensors of each particle and thus obtain the stress field of the middle section of granular gouge for further analysis. Regarding heterogeneity, the variance (or standard deviation) is commonly used as an effective tool to quantitatively measure how scattered, or how heterogeneous, a data group is with respect to the mean. However, the variance is mainly defined and applicable to univariate (or scalar) data. Since stresses in the gouge are tensors, for quantifying the gouge stress field heterogeneity at each instance of time, we employ a concept of variance for stress tensor data – stress dispersion (S_{dis}) – that we have developed earlier (Gao and Harrison, 2018b).

Considering the 2D case here, the stress tensor of each constant strain finite element in the gouge particle is

$$\mathbf{S} = \left[\begin{pmatrix} \sigma_x \\ \tau_{xy} \end{pmatrix} \begin{pmatrix} \tau_{xy} \\ \sigma_y \end{pmatrix} \right] \tag{1}$$

where σ and τ are the normal and shear tensor components, respectively. It has been proved that the variability of stress tensor data can be adequately represented by the variability of their distinct tensor components in a multivariate statistics manner (Gao and Harrison, 2018a); thus, we use the effective variance – a widely used concept in the field of multivariate statistics for group variability comparison (Peña and Rodríguez, 2003) – to measure the overall dispersion of a stress field (S_{dis}) based on the distinct tensor components. For stress tensor $\mathbf{S}$, its distinct tensor components can be expressed by

$$\mathbf{S}_\mathrm{d} = \mathrm{vech}\,(\mathbf{S}) = \begin{bmatrix} \sigma_x & \tau_{xy} & \sigma_y \end{bmatrix}^T \tag{2}$$

where the subscript "d" denotes "distinct", $[\cdot]^T$ represents the matrix transpose, vech$(\cdot)$ is the half-vectorization function that stacks only the lower (or upper) triangular (i.e., on and below the diagonal) columns of a tensor into a column vector containing only the distinct components. The stress dispersion (i.e., effective variance) is then calculated as

$$S_{dis} = \sqrt[\frac{1}{2}m(m+1)]{\det(\mathbf{\Omega})} \tag{3}$$

where m is the dimension of stress tensor ($m = 2$ here), det() is the matrix determinant function, and $\mathbf{\Omega}$ is the covariance matrix of the stress vector $\mathbf{S}_\mathrm{d}$ (Gao and Harrison, 2018b):

$$\mathbf{\Omega} = \mathrm{cov}\,(\mathbf{S}_\mathrm{d}) = \frac{1}{n}\sum_{i=1}^{n} (\mathbf{S}_\mathrm{d} - \overline{\mathbf{S}}_\mathrm{d})(\mathbf{S}_\mathrm{d} - \overline{\mathbf{S}}_\mathrm{d})^T \tag{4}$$

where cov$(\cdot)$ is the covariance function, n is the number of calculated particles, and $\overline{\mathbf{S}}_\mathrm{d}$ denotes the mean stress vector given by

$$\overline{\mathbf{S}}_\mathrm{d} = \frac{1}{n}\sum_{i=1}^{n} \mathbf{S}_\mathrm{d} \tag{5}$$

The stress dispersion (S_{dis}) acts as a tensor version of variance, which gives a scalar-valued measure of gouge stress field heterogeneity, i.e., how spread out the gouge stress field group is with respect to their mean. It has the same unit as the variance of stress components, i.e., the square of the unit of stress. The larger the S_{dis} is, the more heterogeneous the gouge stress field is. The effectiveness of stress dispersion for stress field heterogeneity quantification has been tested and verified systematically in our previous work (Gao and Harrison, 2018b).

2.4. Gouge particle contact change

The center position of each particle is also recorded every 1 ms. Although the particles are allowed to deform, the deformation is several orders smaller than the particle size. For simplicity, we regard particles as circles even after deformation, and two particles are in contact if the distance between their centers is smaller than the sum of their radii (tolerance of 10^{-2} mm is allowed). As such, the contact number of each particle is obtained every 1 ms. If the contact number of a particle changes in a time step, either

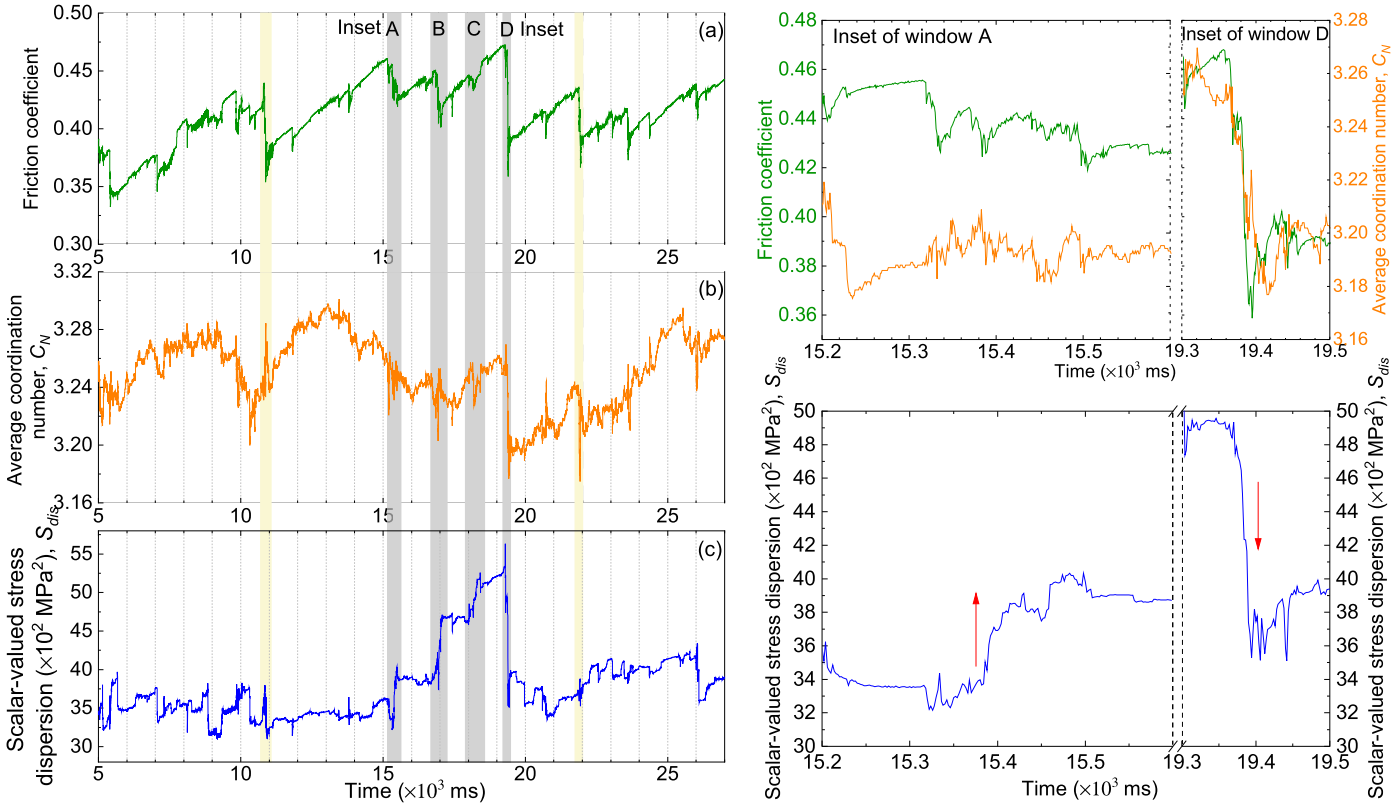

Fig. 2. Characteristic behavior of stick-slip cycles showing (a) the macroscopic friction coefficient, (b) the average coordination number, and (c) the scalar-valued stress dispersion as a function of time. The system before 5,000 ms is not shown. Windows A-D highlighted by the vertical gray shadings correspond to the time span 15.2-15.6, 16.8-17.1, 17.9-18.3, 19.3-19.5 ($\times 10^3$ ms), respectively. C_N shows a similar trend to the macroscopic friction coefficient, as illustrated in the insets of windows A and D on the right panel. The red arrows in the bottom right insets indicate the opposite trends of gouge stress field heterogeneity evolution in windows A and D. The two typical slip events shaded in light yellow are pervasive regime (around 10,900 ms) and dispersive regime (around 21,900 ms), respectively, as will be discussed later in Section 3.2.

in terms of contact loss or contact gain, the particle is regarded as a "contact-changed particle". Such contact change is identified by the ID of the "contact-changed particle", the occurrence time, as well as the contact-change magnitude (how many contacts the particle has changed).

3. Results

3.1. Coordination number and gouge stress heterogeneity

When the macroscopic friction coefficient shows no monotone increase after 5,000 ms, we observe a clear reoccurrence of drop and rise in terms of the macroscopic friction coefficient (Fig. 2a). During the shear, the loss of particle contact inside the gouge often leads to frictional instability (Tordesillas et al., 2010). The coordination number, defined as the number of contacts of a particle with its neighbors, is therefore well correlated with gouge stability (Dorostkar et al., 2017). For example, in a scenario where a large proportion of particles in a system lose their contacts, instability will arise and consequently, yield a smaller coordination number. Here, we use the average coordination number, C_N, to characterize the system instability in terms of contact status, defined as

$$C_N = \frac{\sum_{i=1}^{N} C_i}{N}, \tag{6}$$

where N is the number of particles, C_i is the contact number of particle i.

To quantify the stress field redistribution in the gouge as a consequence of fault slip, we use the scalar-valued measure of the heterogeneity degree of a stress field – stress dispersion (S_{dis}) – by calculations using the stress tensor components of all particles considered (see Section 2.3). To avoid confusion about the different stress terminologies commonly seen in the earthquake literature (e.g., stress drop, shear stress), it is worth noting that here the "stress field heterogeneity" or "stress heterogeneity" refers to the overall stress field distribution condition in the granular gouge (e.g., Fig. 1b) at each instance of time hereafter; the shear force/stress (normalized by the normal force) is indicated by "friction" or the "macroscopic friction coefficient".

We emphasize that the scalar-valued measure of stress heterogeneity, S_{dis}, quantifies the degree of stress heterogeneity of the granular gouge from a "macroscopic" viewpoint, while the average coordination number, C_N, gives a "microscopic" description of gouge connectivity at the particle level. To further probe the connections between the micro- and macro-behaviors, we show C_N and S_{dis} in the granular gouge throughout the shearing history in Fig. 2b and c, respectively. The shaded windows A to D in Fig. 2a-c highlight the typical slip events characterized by relatively large friction drops.

The average coordination number exhibits a similar trend to the macroscopic friction coefficient. During the stick phase, particles tend to move by integrated slipping and rolling, distortion, and local collapse of force chains, corresponding to steady evolutions of C_N (Ciamarra et al., 2010; Hayman et al., 2011; Majmudar and Behringer, 2005). C_N simultaneously manifests striking fluctuations at slip phases (as shown in windows A and D in Fig. 2). Drastic variations of C_N explain the fact that the granular layer undergoes rapid contact rearrangements during slip. The plummet of C_N at failure (inset of window D in Fig. 2) reflects the rapid and significant degeneration of contacts. Of note is that $C_N = 3$ is the nominal jamming transition point for frictional particles in 2D

(Majmudar et al., 2007; Zhang et al., 2010). Our data show that C_N is constantly above 3, suggesting that the system remains jammed during the full stick-slip cycles – we note that localized unjamming may take place, however.

In view of the macroscopic friction coefficient drop during fault slip, one may intuitively expect that the stress field of the gouge would be more evenly distributed, i.e., more homogeneous (Gao et al., 2018, 2019, 2020), because of the release of local stress concentrations along the stress chains (e.g., Fig. 1b). However, we observe two opposite evolution trends of gouge stress heterogeneity during fault slip (bottom right insets in Fig. 2): S_{dis} increases stepwise from windows A to C, with each surge coinciding with the slipping episodes; conversely, S_{dis} plummets in window D characterized by a large drop of macroscopic friction coefficient (Fig. 2a). In other words, the stress field of the gouge becomes more heterogeneous with fault slip in windows A to C, but the subsequent slip event in window D homogenizes the stress field to a tremendous degree. This implies that fault slip is associated with friction drop, but does not necessarily result in a lower degree of gouge stress heterogeneity. Besides, preceding the slip event A, the gouge stress heterogeneity is relatively constant, suggesting that S_{dis} is perhaps an indicator of steady-state conditions.

The idea that fault slip alters the gouge stress state is not new (Ben-Zion, 2001; Ben-Zion et al., 2003). However, very little is known about the mechanisms governing the gouge stress field heterogeneity in the evolution of stick-slip cycles. As implied by the simultaneous drastic fluctuations of C_N and S_{dis} in response to the macroscopic friction coefficient drop, the connections between contact rearrangement and stress redistribution inside the gouge may offer a powerful explanation for the opposite trends of gouge stress field heterogeneity (larger vs. smaller). In what follows, we focus on windows A and D for the analysis of increased and decreased gouge stress field heterogeneity, respectively.

3.2. Two regimes of gouge contact evolution

As can be seen from the insets of Fig. 2, the steeper C_N variation trend in window D implies more significant granular particle contact rearrangement as opposed to that in window A. For quantitative description, in such a small time interval (1 ms) considered, we regard that the contact state of a particle is modified only if its coordination number changes (including both contact loss and contact gain). As such, we extract the information of contact-changed particles, and plot their distributions in the timeline in Fig. 3a. Here, only the magnitude of contact changes is plotted, while the nature (contact loss or contact gain) is not differentiated.

The contact changes of particles occur almost on a fifty-fifty basis between contact loss and contact gain (see Table S2 in Supplementary Material for the statistics of contact-change events). Without differentiating contact loss and contact gain, we classify the contact-change events into three levels by magnitude: level 1 – lose or gain one contact (blue circles in Fig. 3a); level 2 – lose or gain two contacts (orange asterisks in Fig. 3a); level 3 – lose or gain contacts larger than 2 (red stars in Fig. 3a). Fig. 3a shows that most contact-change events are at level 1, as evidenced by the dominancy of blue circles. The population of level 1 events can roughly indicate the magnitude of the macroscopic friction coefficient drop. Specifically, level 1 events align densely and continuously in columns at large macroscopic friction coefficient drops (see windows A and D in Fig. 3a), indicating a strong cause-and-effect relationship between contact rearrangement and instability; while at some small macroscopic friction coefficient drops, level 1 events are distributed in an incompact and intermittent sense vertically (e.g., the black rectangle in Fig. 3a). Level 2 events are about two orders of magnitude less than level 1 and preferentially concentrated along the columns of level 1 events, where large macroscopic friction coefficient drops occur. Level 3 events also exhibit similar spatial aggregation, despite their small population.

A careful comparison of the zoomed-in windows A and D (Fig. 3a right) offers more details: contact changes in window A are intermittently aligned vertically, resembling broken (dashed) lines. Given a continuous rather than discontinuous alignment at an instant of time, all particles undergo contact changes. In fact, none of the distributions is "continuous" as some of them appear to be, and window D is no exception (see Figure S2e in Supplementary Material for the unscaled version). In addition, a general characteristic observed from these distributions is that the vertical alignments are intermittent, although constitutive segments (referred to as "patches" here) in a column look alike in terms of their geometries (zoomed-in window A in Fig. 3a). This similarity makes the main point of our work: contact rearrangement does not occur for all particles at the same instant of time, regardless of the magnitude of friction drop. Instead, initiation of contact rearrangement, which we call "origins", complies with spatial distributions, and these "origins" evolve somehow in the same form (Fig. 3c and d).

We offer a physical explanation of the geometries and distributions of the patches. The population of the patches corresponds to the density of the "origins". The width and height of the patch respectively determine the time span and the range that each "origin" takes effect. By combining patch population and height, more and higher patches indicate that a wider range of the fault is affected by contact rearrangement. If we further consider the time span, the "origin" may expand, shrink, move, or simply remain the same. Reflecting on patch geometries, the height of a patch can increase, decrease, or remain unchanged vs. time (Fig. 3b). Particular attention is paid to the "unchanged" height: a rectangle-like patch, if oriented horizontally, refers to no change of the "origins"; otherwise, any inclination indicates a move of the "origins", i.e., regional migration of contact rearrangement without change in size. However, combinations of the above kinetic regimes could yield more complex shapes.

Now, we understand that the essential differences between different patch alignments reside in their contact rearrangement initiation and migration. Imagine this situation: the "origins" are sparsely distributed, small in size and with little migration (Fig. 3c), and only sparse spots on the fault have been reorganized. These "contact-changed patches", along with their respective energy release, principally contribute to macroscopic friction coefficient drop on the one hand, and the more distinguished stress field with those unchanged regions on the other hand. The latter explains the larger stress heterogeneity of gouge at friction drop. The opposite situation is described by the densely populated, large "origins" with large migration (Fig. 3d). Contact rearrangement initially prevails and then migrates to those unchanged regions, making the contact rearrangement pervasive in the gouge. Upon friction drop, the more homogeneous stress field distribution inside the gouge is a trivial consequence of the fact that the integrated contact network topology has been reorganized.

Referring to the two scenarios described above, the discontinuous alignment with little inclination in window A distinguishes the regions where contact rearrangement occurs and not. Eventually, the areas marked by contact rearrangement are dispersive along the fault. A similar dispersive regime applies to windows B and C. In contrast, each patch in window D appears much thicker and more inclined from the very beginning (Figure S2e in Supplementary Material), and thus can be illustrated by the pervasive regime. Nevertheless, the opposite effects of the dispersive and pervasive regimes on gouge stress field heterogeneity may be more complex than that just described, because there is no exact extent to which the contact rearrangement is regarded as pervasive.

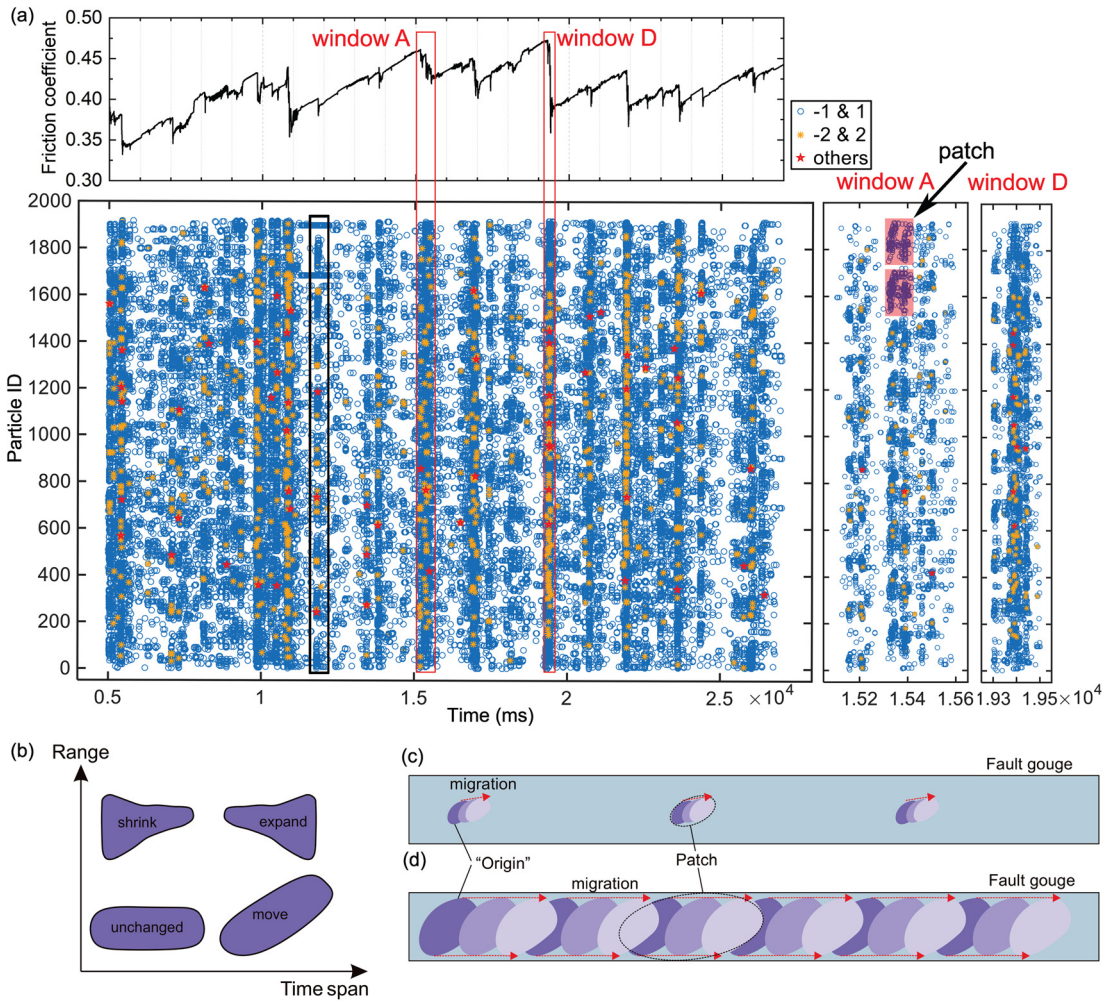

Fig. 3. (a) Particles with contact change in the timeline. The particles having no contact change are not shown. In the legend, negative and positive values respectively denote contact loss and contact gain, but are not differentiated in color; the number refers to the number of contact loss/gain. Say, "−1 & 1" in the legend denotes the particles with one contact loss/gain. "Others" includes those larger than 2 or smaller than −2 (e.g., −3, 3 and −4, 4). The black rectangle shows a vertical alignment in an incompact and intermittent sense. Zoomed-in windows A and D on the right are scaled with time. The unscaled windows A to D refer to Figure S2 in Supplementary Material. (b) The physical meaning of patch geometries. Decreasing and increasing height denotes a shrinking and expanding range of contact rearrangement, respectively (top two). A rectangle-like shape in horizontal orientation means no change in range, while its inclination corresponds to the move of the origin (aka, regional migration without changes in size) (bottom two). (c) and (d) Two-end member regimes of dispersive vs. pervasive contact rearrangement, respectively. Note that the time effect is not incorporated in the two regimes.

One should note that it accounts for nothing to focus on one column of patches, as they occur at an instant of time and the gouge stress field redistribution in a slip event is the product of several instants of time. What makes a difference is the competition between the "dispersive" and "pervasive" columns. That is, local fluctuations should never be confused with the overall trend. Take window B as an example, S_{dis} in fact experiences an instantaneous drop at $t = 1.695 \times 10^4$ ms (Figure S2c in Supplementary Material) due to the quite pervasive contact rearrangement at that moment.

We now understand that it is the "dispersive" or "pervasive" contact arrangement that makes the stress dispersion larger or smaller. To distinguish the two regimes more quantitatively, the particle velocity distributions in the shear direction (horizontal velocity) in four dispersive regimes (windows A-C and the slip event around $t = 21{,}900$ ms) characterized by friction coefficient drop and increased stress dispersion (Fig. 2a and c) are shown in Fig. 4a-d, and those in two pervasive regimes (window D and the slip event around $t = 10{,}900$ ms) characterized by friction coefficient drop and decreased stress dispersion (Fig. 2a and c) are presented in Fig. 4e-f. For the dispersive regime cases shown in Fig. 4a-d, most particles have no/little movement, while only a small portion of them move in both the shear and anti-shear directions, causing mainly local contact arrangements. While for the pervasive regime cases shown in Fig. 4e-f, nearly all of them are active. The significant variation in particle velocities, in terms of direction and magnitude, explains that almost all the particle-particle contacts have been modified in the pervasive regime.

3.3. Temporal effects of contact rearrangement

The above explains two different regimes of granular gouge instability regarding the spatial range of contact rearrangement, irrespective of the timescale for this to happen. However, the coupling of scale and time could produce complex patch geometries. We now focus on the temporal characteristics of the dispersive and pervasive regimes to further elaborate their spatio-temporal evolutions. To quantify the degree of contact rearrangement, we calculate the number of "contact-changed particles" (see Section 2.4). Again, neither the magnitude nor the nature of the contact changes is considered in the calculation. Fig. 5a clearly shows that window D involves the most particles in contact rearrangement. However, this comparison gives little idea about the impact of these particles. To omit the influence of particle number, we introduce a

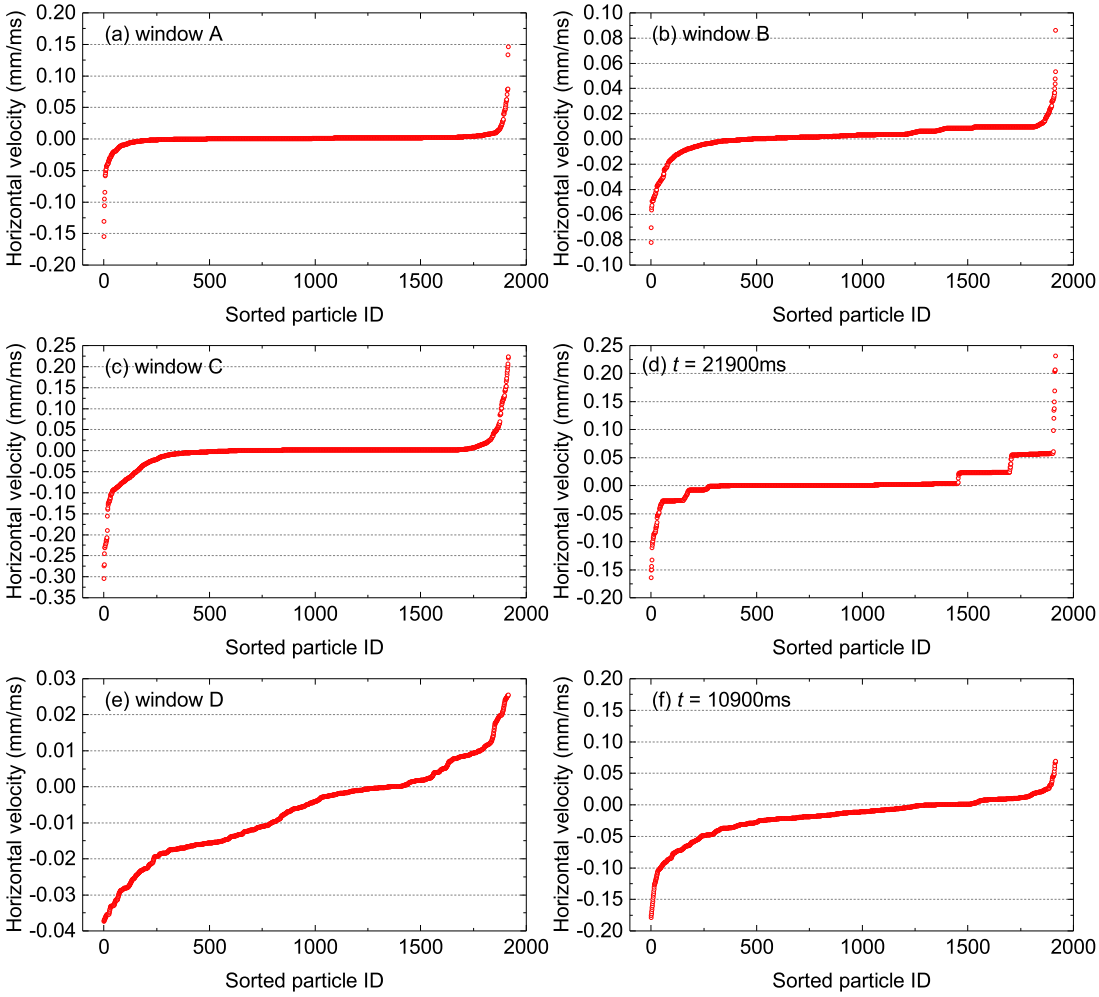

Fig. 4. Horizontal velocity distributions in four dispersive regimes: (a) window A ($t = 15{,}200$ ms), (b) window B ($t = 16{,}950$ ms), (c) window C ($t = 18{,}200$ ms), and (d) the slip event around $t = 21{,}900$ ms; and in two pervasive regimes (e) window D ($t = 19{,}400$ ms), and (f) the slip event around $t = 10{,}900$ ms. Particle velocities are sorted in ascending order, so the sorted particle ID has no relevance to their real ID. The slip events around $t = 10{,}900$ ms and $t = 21{,}900$ ms correspond to the light yellow shadings in Fig. 2a.

linkage effect index χ to quantify the overall effect of contact-changed particles on contact rearrangement, defined as

$$\chi = \begin{cases} (N_{t+1} - N_t)/N_t, & N_t \neq 0 \\ N_{t+1}, & N_t = 0 \end{cases}, \tag{7}$$

where N is the number of contact-changed particles, t and $t+1$ denote two successive time stamps.

Now, we explain the physical meaning of χ with respect to patch geometries as described in Fig. 3b. $\chi = 0$ means that the range size of contact reorganization has no change with time, corresponding to the fact that the "origins" keep unchanged or move (regional migration). Positive and negative values of χ denote an expanding and shrinking range, respectively. The absolute value measures the expanding/shrinking rate. The scale-free linkage effect χ can be explained such that, one contact-changed particle will involve three particles in the following contact rearrangement ($\chi = 2$), or 100 contact-changed particles will expand to the range of 300 particles.

For window D recognized as the pervasive regime, we have observed contact reorganization of a large number of particles in a very short time span (Fig. 5a), which is reminiscent of the expanding origins. We, therefore, expect that these particles with contact change would affect more others, i.e., a large linkage effect. However, our speculation is not supported by Fig. 5b. Surprisingly, window A seems to have a larger linkage effect than window D.

To evaluate the linkage effect more quantitatively, we plot the probability density distributions of χ in Fig. 5c. The four distributions are virtually indistinguishable, and decay exponentially to the background level at around 5. In order to see the details in the decaying phase, the probability density distributions of χ are plotted on a much finer scale (see inset of Fig. 5c). For the four windows, the χ corresponding to the maximum probabilities almost coincide at the value very close to 0 (the triangle markers in the inset of Fig. 5c). Recalling the fact that $\chi = 0$ means that the range size of contact reorganization has no change with time, "origins" of the four windows tend to keep unchanged or move (neither shrink nor expand). Relatively speaking, window D has the least probability among others at this near-zero value, implying its difficulty to maintain the size of "origins" or to move. Referring to Figure S2e in Supplementary Material, the "origins" in window D are moving, as evidenced by the inclination shape of contact-changed patches. Therefore, the "difficulty" principally stems from the less capability of keeping the "origin" size. The significant preference for the negative region also indicates the shrinking "origins" in window D. For the positive region, windows A to C exhibit two peaks at the interval (1, 3), while window D is hard to follow the trend. It can be interpreted that the "origins" in window D lose the capability to expand in a fast manner.

The combination of Fig. 5a and c makes another point of this work: "origins" in window D are much larger and migrate faster,

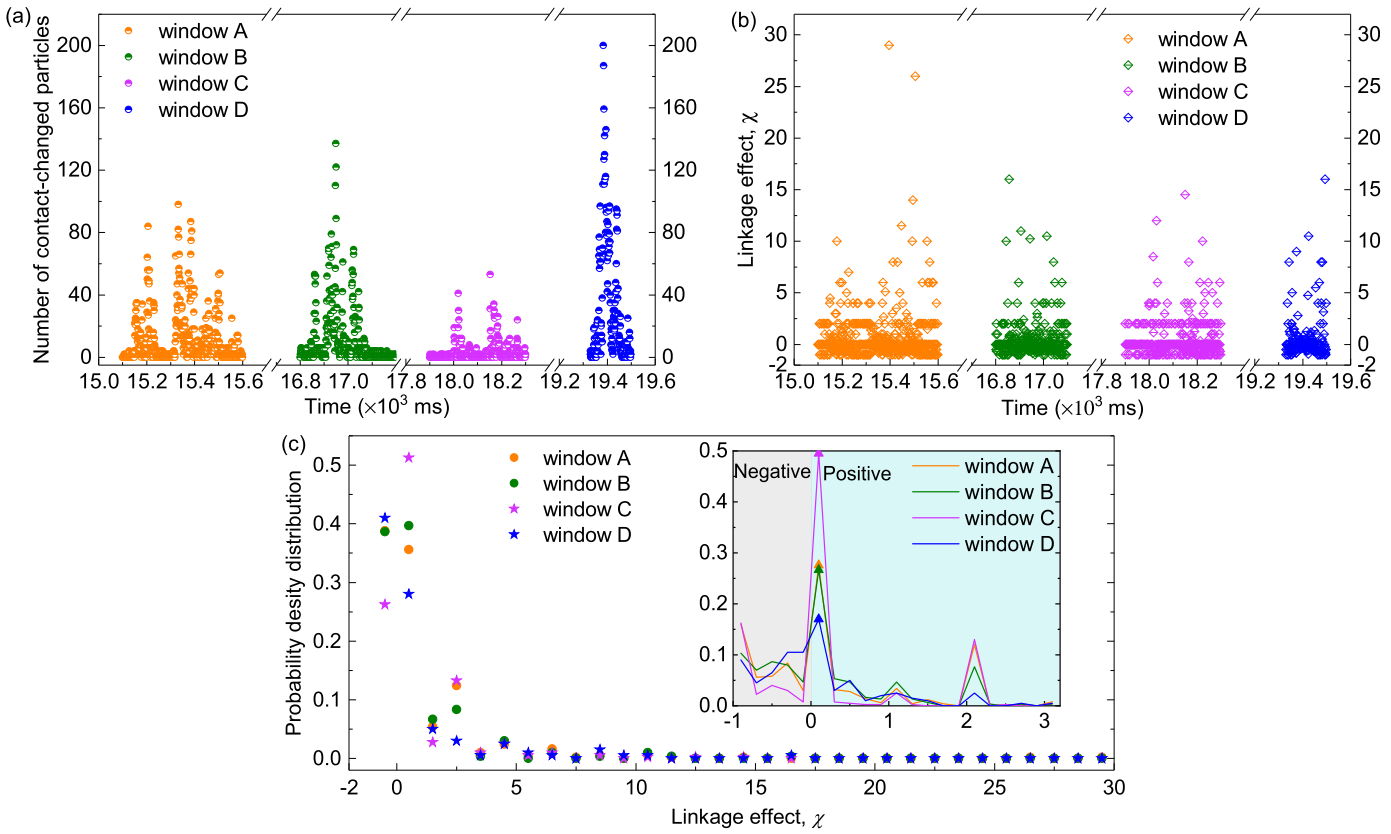

Fig. 5. (a) Number of particles with contact change. (b) Linkage effect of contact rearrangement. Negative values denote a decreasing trend of the linkage effect. (c) Probability distribution of the linkage effect.

but the influence is diminishing. Although contact rearrangement initiates in smaller sizes of "origins" in windows A to C, their "origins" are more likely to grow larger. The fact that fewer particles take greater effects in the vicinity tells us that contact rearrangement initiates from the key positions in the contact network. Recalling the stress chain theory (Anthony, 2005; Peters et al., 2005; Zhang et al., 2014), some key particles are supporting the contact structure. In the dispersive regime, the key contacts are reorganized, leading to a larger gouge stress heterogeneity. The rearranged contact structure produces new key contacts, which play the leading role in the next dispersive regime of contact reorganization. Therefore, system instability in the dispersive regime is induced by local contact rearrangement, and accumulates stress heterogeneity consequentially. However, with the accumulation of gouge stress heterogeneity, the system will eventually fall into instability via pervasive contact reorganization. In this sense, we can regard the macroscopic friction coefficient drop governed by a dispersive regime as the preparation process for a slip event in a pervasive regime.

4. Limitations, discussion and conclusions

The numerical model is constructed based on the laboratory photoelastic experiment conducted by Geller et al. (2015), in which the photoelastic plates used as the ambient "intact" rocks were not strong enough to sustain large normal loads. Despite the small normal load with respect to the geological context, both the plates and particles have deformed a lot (i.e., not infinitesimal strain) during the shear, given the mechanical parameters used in the FDEM model (see Table S1 in the Supplementary Material) and the capability of FDEM for large deformation simulation. This type of material can be deemed as similitude material, which is commonly used in laboratory-scale friction experiments (Xia et al., 2004) and can be upscaled to in situ conditions through particular law of similitude. However, the rate and state friction law applies to both fault gouges and bare rock surfaces, but the latter are not described by the current model. We are not confident at the moment about how our numerical model could be upscaled to natural faults.

Considering the fact that the deformations of granular particles are much smaller than their size (Radjai et al., 1996), we abstract the granular gouge into an unweighted contact force network. Contact force configuration during shearing is deciphering the evolving stability as it responds to external loads (Tordesillas et al., 2010). The "response" generally includes integrated network deforming and catastrophic contact reorganization. The former is common during the stick phase, in connection with interseismic frictional healing. Contact reorganization usually corresponds to the transition from stick to slip phases.

From a more fundamental point of view, the evolution of contact rearrangement can be interpreted as a phase transition process. The competition between long-range interaction and system disorder determines the nature of the transition (first-order or second-order). Here, system disorder is mainly controlled by gouge structure or stress heterogeneity. In the case of limited disorder, localized damage occurs by nucleation of dynamic clusters (expanding of "origins"), analogous to the first-order phase transition with a non-diverging correlation length. When initial disorder dominates the interaction, such as in the percolation problem, the sizes of patches are expected to show a diverging correlation length as evidenced by the fast movement of "origins", arguing for a second-order transition. The system dominated by interaction and disorder explains the regime of fictional instability governed by dispersive and pervasive regimes, respectively. Ben-Zion (2001) also pointed out that the degree of disorder in fault heterogeneities is a governing parameter of the dynamics.

However, driven by increasing entropy, a self-organized system evolves into a highly distorted state characterized by strong stress field heterogeneity. In this sense, the accumulation of stress field heterogeneity is an evitable consequence of the increase in entropy in a large earthquake cycle, which eventually destroys the long-range stress correlations and resets the beginning of a new cycle (Ben-Zion, 2001). Such two distinguishable regimes seem rare for natural faults where a mixed regime may prevail. Nevertheless, our analysis may suggest that accumulated gouge stress heterogeneity in seismic faulting is indicative of several cycles of seismic events followed by a large earthquake in the future.

CRediT authorship contribution statement

All authors have contributed to the work, approved the manuscript and agreed on its submission: Ke Gao performed the numerical simulation and revised the manuscript. Yahui Zhang performed the analysis of the numerical results and wrote the manuscript. Changdong Li contributed to revising the manuscript.

Declaration of competing interest

The authors declare that they have no known competing financial interests or personal relationships that could have appeared to influence the work reported in this paper.

Data availability

Data will be made available on request.

Acknowledgements

This work is supported by the National Key R&D Program of China (2022YFF0800601). Changdong Li would like to acknowledge the financial support of the National Natural Science Fund for Major Programs of China (42090054), and the National Natural Science Fund for Excellent Young Scholars of China (41922055). The authors would like to thank Dr. Paul A. Johnson from the Los Alamos National Laboratory for the constructive comments and suggestions.

Appendix A. Supplementary material

Supplementary material related to this article can be found online at https://doi.org/10.1016/j.epsl.2023.118086.

References

Anthony, J.L., 2005. Influence of particle characteristics on granular friction. J. Geophys. Res. 110. https://doi.org/10.1029/2004jb003399.
Beeler, N., Tullis, T., Weeks, J., 1994. The roles of time and displacement in the evolution effect in rock friction. Geophys. Res. Lett. 21, 1987–1990.
Ben-Zion, Y., 2001. Dynamic ruptures in recent models of earthquake faults. J. Mech. Phys. Solids 49, 2209–2244.
Ben-Zion, Y., Eneva, M., Liu, Y., 2003. Large earthquake cycles and intermittent criticality on heterogeneous faults due to evolving stress and seismicity. J. Geophys. Res., Solid Earth 108. https://doi.org/10.1029/2002jb002121.
Brace, W., Byerlee, J., 1966. Stick-slip as a mechanism for earthquakes. Science 153, 990–992.
Byerlee, J.D., Brace, W., 1968. Stick slip, stable sliding, and earthquakes—effect of rock type, pressure, strain rate, and stiffness. J. Geophys. Res. 73, 6031–6037.
Ciamarra, M.P., Lippiello, E., Godano, C., de Arcangelis, L., 2010. Unjamming dynamics: the micromechanics of a seismic fault model. Phys. Rev. Lett. 104, 238001.
Dieterich, J.H., 1978. Time-dependent friction and the mechanics of stick-slip. In: Rock Friction and Earthquake Prediction. Springer, pp. 790–806.
Dieterich, J.H., 1979. Modeling of rock friction: 1. Experimental results and constitutive equations. J. Geophys. Res., Solid Earth 84, 2161–2168.
Dorostkar, O., Guyer, R.A., Johnson, P.A., Marone, C., Carmeliet, J., 2017. On the micromechanics of slip events in sheared, fluid-saturated fault gouge. Geophys. Res. Lett. 44, 6101–6108.
Falk, M.L., Langer, J.S., 1998. Dynamics of viscoplastic deformation in amorphous solids. Phys. Rev. E 57, 7192.
Ferdowsi, B., 2014. Discrete element modeling of triggered slip in faults with granular gouge: application to dynamic earthquake triggering. ETH-Zürich, Switzerland.
Ferdowsi, B., Griffa, M., Guyer, R., Johnson, P., Marone, C., Carmeliet, J., 2013. Microslips as precursors of large slip events in the stick-slip dynamics of sheared granular layers: a discrete element model analysis. Geophys. Res. Lett. 40, 4194–4198.
Ferdowsi, B., Griffa, M., Guyer, R.A., Johnson, P.A., Marone, C., Carmeliet, J., 2014. Three-dimensional discrete element modeling of triggered slip in sheared granular media. Phys. Rev. E 89, 042204.
Gao, K., Euser, B.J., Rougier, E., Guyer, R.A., Lei, Z., Knight, E.E., Carmeliet, J., Johnson, P.A., 2018. Modeling of stick-slip behavior in sheared granular fault gouge using the combined finite-discrete element method. J. Geophys. Res., Solid Earth 123, 5774–5792.
Gao, K., Guyer, R., Rougier, E., Ren, C.X., Johnson, P.A., 2019. From stress chains to acoustic emission. Phys. Rev. Lett. 123, 048003.
Gao, K., Guyer, R.A., Rougier, E., Johnson, P.A., 2020. Plate motion in sheared granular fault system. Earth Planet. Sci. Lett. 548, 116481.
Gao, K., Harrison, J.P., 2018a. Multivariate distribution model for stress variability characterisation. Int. J. Rock Mech. Min. Sci. 102, 144–154. https://doi.org/10.1016/j.ijrmms.2018.01.004.
Gao, K., Harrison, J.P., 2018b. Scalar-valued measures of stress dispersion. Int. J. Rock Mech. Min. Sci. 106, 234–242.
Geller, D.A., Ecke, R.E., Dahmen, K.A., Backhaus, S., 2015. Stick-slip behavior in a continuum-granular experiment. Phys. Rev. E 92, 060201.
Gutenberg, B., Richter, C.F., 1955. Magnitude and energy of earthquakes. Nature 176, 795. https://doi.org/10.1038/176795a0.
Hayman, N.W., Ducloué, L., Foco, K.L., Daniels, K.E., 2011. Granular controls on periodicity of stick-slip events: kinematics and force-chains in an experimental fault. Pure Appl. Geophys. 168, 2239–2257.
Helmstetter, A., Shaw, B.E., 2009. Afterslip and aftershocks in the rate-and-state friction law. J. Geophys. Res., Solid Earth 114.
Im, K., Elsworth, D., Marone, C., Leeman, J., 2017. The impact of frictional healing on stick-slip recurrence interval and stress drop: implications for earthquake scaling. J. Geophys. Res., Solid Earth 122, 10,102–110,117.
Johnson, P.A., Savage, H., Knuth, M., Gomberg, J., Marone, C., 2008. Effects of acoustic waves on stick–slip in granular media and implications for earthquakes. Nature 451, 57–60.
Johnson, T., Wu, F.T., Scholz, C.H., 1973. Source parameters for stick-slip and for earthquakes. Science 179, 278–280.
Kaproth, B.M., Marone, C., 2013. Slow earthquakes, preseismic velocity changes, and the origin of slow frictional stick-slip. Science 341, 1229–1232.
Kruyt, N.P., Rothenburg, L., 2016. A micromechanical study of dilatancy of granular materials. J. Mech. Phys. Solids 95, 411–427. https://doi.org/10.1016/j.jmps.2016.01.019.
Lei, Z., Rougier, E., Knight, E.E., Munjiza, A.A., Viswanathan, H., 2016. A generalized anisotropic deformation formulation for geomaterials. Comput. Part. Mech. 3, 215–228. https://doi.org/10.1007/s40571-015-0079-y.
Li, Q., Tullis, T.E., Goldsby, D., Carpick, R.W., 2011. Frictional ageing from interfacial bonding and the origins of rate and state friction. Nature 480, 233–236.
Mair, K., Frye, K.M., Marone, C., 2002. Influence of grain characteristics on the friction of granular shear zones. J. Geophys. Res., Solid Earth 107, ECV 4-1–ECV 4-9.
Majmudar, T., Sperl, M., Luding, S., Behringer, R.P., 2007. Jamming transition in granular systems. Phys. Rev. Lett. 98, 058001.
Majmudar, T.S., Behringer, R.P., 2005. Contact force measurements and stress-induced anisotropy in granular materials. Nature 435, 1079–1082.
Marone, C., 1998. The effect of loading rate on static friction and the rate of fault healing during the earthquake cycle. Nature 391, 69–72.
Marone, C., Raleigh, C.B., Scholz, C., 1990. Frictional behavior and constitutive modeling of simulated fault gouge. J. Geophys. Res., Solid Earth 95, 7007–7025.
Marsan, D., 2006. Can coseismic stress variability suppress seismicity shadows? Insights from a rate-and-state friction model. J. Geophys. Res., Solid Earth 111.
Munjiza, A., Rougier, E., John, N.W.M., 2006. MR linear contact detection algorithm. Int. J. Numer. Methods Eng. 66, 46–71. https://doi.org/10.1002/nme.1538.
Munjiza, A.A., 1992. Discrete Elements in Transient Dynamics of Fractured Media. Swansea University.
Munjiza, A.A., 2004. The Combined Finite-Discrete Element Method. John Wiley & Sons.
Munjiza, A.A., Knight, E.E., Rougier, E., 2011. Computational Mechanics of Discontinua. John Wiley & Sons.
Munjiza, A.A., Rougier, E., Knight, E.E., 2014. Large Strain Finite Element Method: A Practical Course. John Wiley & Sons.
Nakatani, M., 2001. Conceptual and physical clarification of rate and state friction: frictional sliding as a thermally activated rheology. J. Geophys. Res., Solid Earth 106, 13347–13380.
Peña, D., Rodríguez, J., 2003. Descriptive measures of multivariate scatter and linear dependence. J. Multivar. Anal. 85, 361–374.

Peters, J.F., Muthuswamy, M., Wibowo, J., Tordesillas, A., 2005. Characterization of force chains in granular material. Phys. Rev. E, Stat. Nonlinear Soft Matter Phys. 72, 041307. https://doi.org/10.1103/PhysRevE.72.041307.

Radjai, F., Jean, M., Moreau, J.-J., Roux, S., 1996. Force distributions in dense two-dimensional granular systems. Phys. Rev. Lett. 77, 274.

Rubin, A.M., 2008. Episodic slow slip events and rate-and-state friction. J. Geophys. Res., Solid Earth 113.

Ruina, A., 1983. Slip instability and state variable friction laws. J. Geophys. Res., Solid Earth 88, 10359–10370. https://doi.org/10.1029/JB088iB12p10359.

Scholz, C.H., 1998. Earthquakes and friction laws. Nature 391, 37–42.

Thøgersen, K., Gilbert, A., Schuler, T.V., Malthe-Sørenssen, A., 2019. Rate-and-state friction explains glacier surge propagation. Nat. Commun. 10, 1–8.

Tordesillas, A., Walker, D.M., Lin, Q., 2010. Force cycles and force chains. Phys. Rev. E 81, 011302.

Xia, K., Rosakis, A.J., Kanamori, H., 2004. Laboratory earthquakes: the sub-Rayleigh-to-supershear rupture transition. Science 303, 1859–1861.

Xing, Y., Zheng, J., Li, J., Cao, Y., Pan, W., Zhang, J., Wang, Y., 2021. X-ray tomography investigation of cyclically sheared granular materials. Phys. Rev. Lett. 126, 048002. https://doi.org/10.1103/PhysRevLett.126.048002.

Zhang, J., Majmudar, T., Tordesillas, A., Behringer, R., 2010. Statistical properties of a 2D granular material subjected to cyclic shear. Granul. Matter 12, 159–172.

Zhang, L., Wang, Y., Zhang, J., 2014. Force-chain distributions in granular systems. Phys. Rev. E 89, 012203.

Zheng, J., Xing, Y., Yuan, Y., Li, Z., Zeng, Z., Zhang, S., Yuan, H., Tong, H., Xia, C., Kob, W., 2021. Influence of roughness on granular avalanches. arXiv preprint. arXiv:2107.13927.